Regional Impact of Ozone Precursor Emissions on NOx and O3 Levels at ZOTTO Tall Tower in Central Siberia

Konstantin B Moiseenko[1], Anastasia V Vasileva[1], Andrey I Skorokhod[1], Igor B Belikov[1], and Yury A Shtabkin[1]

[1]Obukhov Institute of Atmospheric Physics

November 26, 2022

Abstract

Seasonal variations of the near-surface odd nitrogen (NO_X=NO+NO_2) and ozone (O_3) mixing ratios at Zotino Tall Tower (ZOTTO), a remote site in central Siberia, are described for years 2007–2014. Conditional probability function analysis and back trajectories are used to determine the origins of clean (continental background, CB) and regional emissions-influenced air. High NO_X levels at the site are observed for air from industrial regions of western Siberia and Ural Mountains, whereas CB air originates from remote areas of North Eurasia within 55°–70°N. The estimated annual means of daytime O_3 and NO_X mixing ratios for CB air are 27.0 ppbv and 0.44 ppbv, correspondingly, vs. the similar quantities of 27.9 and 0.79 ppbv for all data. Monthly ozone for CB air shows a distinct maximum in April, as is the case for Northern Hemisphere midlatitude background (NHMLB) air at the European inflow boundary according to the surface ozone data for Mace Head and Norwegian monitoring sites, and a minimum in late summer – early autumn reflecting a weak continental-scale ozone production from biogenic sources of ozone precursors and wildfire emissions throughout a warm season. During spring and early summer under hot weather conditions, regional anthropogenic and wildfire emissions are an important source for ozone in the continental boundary layer over southern and central Siberia, resulting in surface ozone levels compared to or larger than those observed in NHMLB air. Throughout the remaining part of a year, the central North Eurasia represents a sink for tropospheric ozone on a hemispheric scale.

1 **Regional Impact of Ozone Precursor Emissions on NOx and O3 Levels at ZOTTO**

2 **Tall Tower in Central Siberia**

3 **K. B. Moiseenko[1], A. V. Vasileva[1], A. I. Skorokhod[1], I. B. Belikov[1], and Yu. A. Shtabkin[1]**

4 [1]A.M. Obukhov Institute of Atmospheric Physics, Russian Academy of Sciences, Moscow,

5 119017, Russia

6 Corresponding author: Konstantin Moiseenko (konst.dvina@gmail.com)

7 **Key Points:**

8 • Seasonal variations of NO_X and O_3 at ZOTTO in Siberia show a signature of weakly

9   polluted air throughout a year due to the regional pollution

10 • Origins of clean and polluted air for the site are identified; seasonal cycle of the baseline

11   ozone for central North Eurasia is estimated

12 • In spring–summer, anthropogenic and fire emissions in Siberia provide a net source for

13   tropospheric ozone on regional and hemispheric scales

14 **Abstract**

15 Seasonal variations of the near-surface odd nitrogen ($NO_X=NO+NO_2$) and ozone (O_3) mixing

16 ratios at Zotino Tall Tower (ZOTTO), a remote site in central Siberia, are described for years

17 2007–2014. Conditional probability function analysis and back trajectories are used to determine

18 the origins of clean (continental background, CB) and regional emissions-influenced air. High

19 NO_X levels at the site are observed for air from industrial regions of western Siberia and Ural

20 Mountains, whereas CB air originates from remote areas of North Eurasia within 55°–70°N. The

21 estimated annual means of daytime O_3 and NO_X mixing ratios for CB air are 27.0 ppbv and 0.44

22 ppbv, correspondingly, vs. the similar quantities of 27.9 and 0.79 ppbv for all data. Monthly

23 ozone for CB air shows a distinct maximum in April, as is the case for Northern Hemisphere

24 midlatitude background (NHMLB) air at the European inflow boundary according to the surface

25 ozone data for Mace Head and Norwegian monitoring sites, and a minimum in late summer –

26 early autumn reflecting a weak continental-scale ozone production from biogenic sources of

27 ozone precursors and wildfire emissions throughout a warm season. During spring and early

28 summer under hot weather conditions, regional anthropogenic and wildfire emissions are an

29 important source for ozone in the continental boundary layer over southern and central Siberia,

30 resulting in surface ozone levels compared to or larger than those observed in NHMLB air.

31 Throughout the remaining part of a year, the central North Eurasia represents a sink for

32 tropospheric ozone on a hemispheric scale.

1 Introduction

34   Measurements of ozone (O_3) and its precursors, including odd nitrogen species

35 ($NO_X=NO+NO_2$), allow assessment of the current state of the tropospheric photochemical

36 system (TPS), as well as long-term trends in chemical air composition associated with the

37 changing climate and strength of air pollution sources. Ozone is a key compound of the TPS,

38 whose photolysis initiates most of the chemical reactions through generating an excited atomic

39 oxygen $O(^1D)$. A subsequent reaction of $O(^1D)$ with a molecule of water (H_2O) is the principal

40 source for the tropospheric hydroxyl radical OH which drives oxidation of relatively stable

41 ozone precursor species (e.g., carbon monoxide (CO), methane (CH_4), and heavier hydrocarbons

42 (NMHC)) emitted from various natural and anthropogenic sources. Also, O_3 is an important

43 secondary pollutant whose mixing ratios above 40–60 ppbv are harmful to human health

44 (Atkinson et al., 2016; Kotelnikov et al., 2017; Turner et al., 2016), crops (Fuhrer, 2009;

45 Hollaway et al., 2012; Mills et al., 2007), and natural vegetation (Arnold et al., 2018; Cailleret et

46 al., 2018; Mills et al., 2011, and references therein). Finally, ozone is a climatically important

47 species affecting carbon sequestration and ecosystem hydrology (Felzer et al., 2009). Oxidation

48 of CO, CH_4, and NMHC in the atmosphere occurs via chemical chain reactions with NO_X, which

49 is the rate-limiting precursor in relatively unpolluted air (Kleinman et al., 1997; Lin, 1988),

50 whereas chemical sink of NO_X into more stable reactive nitrogen species (e.g., nitric acid

51 (HNO_3), alkyl, multifunctional organic nitrates, etc.) and their subsequent removal from the

52 atmosphere through deposition and hydrolysis limit the lifetime of NO_X in the lower troposphere

53 by a few hours or days (Browne & Cohen, 2012; Kenagy et al., 2018; Liu et al., 2016), thus

54 limiting total ozone production on a regional scale. Hence, observations of O_3 and NO_X levels in

55 background air far from local pollution sources allow for some conclusions on the overall

56 abundance of secondary pollutants in the air and the net ozone production potential of the

57 regional pollutant emissions. From this point of view, simultaneous measurements of the above

58 species at remote continental and marine sites are of special interest, being representative for

59 large geographical areas and characterizing some features of the reference state TPS (Derwent et

60 al., 1998; Oltmans, 1981; Parrish et al., 2013; Singh et al., 1978).

61 In the present study, we describe the seasonal cycles of O_3 and NO_X at Zotino Tall Tower

62 Observatory (ZOTTO) (Heimann et al., 2014; Kozlova & Manning, 2009), a remote station in

63 central Siberia that has been put into operation in October 2006, as a joint project between the

64 Max Planck Institute of Biogeochemistry, Jena (Germany), and the I. V. Sukachev Institute of

65 Forest, Siberian Branch of the Russian Academy of Sciences, Krasnojarsk (Russia). The site is

66 perfectly placed to study ozone photochemistry in the continental boundary layer (CBL) under

67 background and polluted conditions. Spatial localization of major source regions for odd

68 nitrogen and ozone is performed through the Conditional Probability Function analysis

69 (Ashbaugh et al., 1985, Vasconcelos et al., 1996) coupled with 3-day Lagrangian (kinematic)

70 back trajectories to determine the origins of clean and polluted air for ZOTTO. Ozone levels for

71 the continental background (CB) and regional emissions-influenced (REI) air masses are then

72 analyzed to quantify the impact of regional pollution sources on the abundance of ozone in the

73 lower troposphere over remote North Eurasia and assess the importance of Siberia as a net sink

74 or source for tropospheric ozone on continental and hemispheric scales.

75 **2 Data Sets and Analysis**

76 2.1 The ZOTTO site

77 The research site (http://www.zottoproject.org) (60° 48′ N, 89° 21′ E, 114 m asl) is

78 located in central Siberia on the eastern edge of the West Siberian Lowland, ~ 20 km west of the

79 Zotino settlement on the Yenisey River (star symbol in Figure 1). The surrounding vegetation is

80 a mixture of bogland and boreal coniferous forest. The local climate is strongly continental with

81 a large seasonal temperature tendency from > 30°C in summer to < -40°C in winter. The

82 climatological wind rose at the nearby weather station shows an appreciable change in direction

83 of the prevailing winds from S and SW in winter to the NW quadrant in summer, reflecting

84 seasonal variations in circulation patterns over Siberia (Eneroth et al., 2003; Heimann et al.,

85 2014). Consequently, the most significant sources of atmospheric contamination affecting the

86 site are large towns and industry in West Siberia (~ 500–1000 km SSE to NW from the site) as

87   well as steppe and forest fires in northern Kazakstan and southern Siberia (Chi et al., 2013;

88   Michailov et al., 2017; Thorp et al., 2020). On a yearly basis, relatively clean air is measured at

89   the site for approximately half of the time, with the longest periods of near-pristine conditions

90   observed in summer months due to the seasonal shift in the prevailing air transport pathways to

91   the northern latitudes and the shorter atmospheric residence times of pollutant species in CBL in

92   this period of a year (Michailov et al., 2017).

93   2.2 NO_X and O_3 data

94   Ozone was measured with Dasibi 1008-AH or 1008-RS UV photometric gas analyzers

95   having a measurement range of 1–1000 ppbv and an estimated precision of the original 1-min

96   data of ~ 1 ppbv at ozone levels well above the detection limit. Nitrogen oxides were measured

97   with Thermo Fisher Scientific TE42C-TL instrument. The method is based on the luminescence

98   radiation from the chemical reaction between NO and O_3. To measure NO_2, a catalytic converter

99   reducing NO_2 to NO was used. The instrument has a response time of 60 sec and overall

100   uncertainty of ±1% for measured NO and NO_2 mixing ratios well above the detection limit of

101   0.05 ppbv. The 1-min O_3, NO, and NO_2 data were filtered for spurious impact of local pollution

102   sources seen as strong short-period fluctuations in the measured species mixing ratios (93% of

103   data capture). The filtered data have been aggregated to 1-hour averages centered at 00:00,

104   01:00, …, 23:00 UTC provided both O_3 and NO_X data cover at least half of the respective hour.

105   The afternoon means (12:00–17:00 local time) of hourly NO_X and O_3 mixing ratios for the whole

106   observation period from March 2007 to December 2014, which are further referred to as *daily*

107   *data*, are used to study the O_3–NO_X correlations and source-receptor relationships for the site.

108   The daily mixing ratios seem to be most appropriate for characterizing the combined effect of

109   vertical mixing in the boundary layer and photochemistry during sunlight hours, the processes

110   which are not separated straightforwardly based on the present observations.

111   2.3 Trajectrory model

112   Ensembles of three-dimensional five-day backward Lagrangian air parcel trajectories

113   were generated with the earlier developed computational code (Vasileva et al., 2011), which

114   utilizes the ERA-Interim 0.75º×0.75º 6-hour meteorological data. For each day, the calculations

115   were conducted every hour from 00:00 to 23:00 starting from pressure levels of 950, 925, 900,

116 and 875 hPa (400–1000 m agl at ZOTTO) by varying additionally the ground location (the

117 ZOTTO coordinates ±0.25º latitude or longitude), with the trajectory segment endpoints saved at

118 the Δ_t = 30 min time increment. The above range of starting (in backward direction) altitudes is

119 chosen to constrain the regional pattern of low-level air mass transport, to which the results of

120 the present source-receptor analysis are found to be most sensitive. Varying trajectory duration

121 time (τ_t) from 2 to 5 days or limiting the range of starting heights to 950–900 hPa does not lead

122 to any appreciable change in our final estimates, so below we discuss the results of simulations

123 for the optimal value of τ_t = 3 days, as it provides the best agreement between the model-

124 predicted source area for the site and the regional pattern of anthropogenic and wildfire NO_X

125 emissions.

126   2.4 Source – receptor relationship

127   Air masses arriving at ZOTTO have been sorted into *clean* and *polluted* categories

128 according to the measured NO_X levels. Subtracting the median of daily $[NO_X]$ values (here and

129 after, $[\cdot]$ is a species mixing ratio in ppbv) in the ±15 days running window from the original

130 data, we obtain a *synoptic* part of the NO_X time series (NO_X'), containing short-term variations

131 with the periods of 2–30 days. The NO_X' component resembles the stationary sequence with no

132 pronounced long-term variations and trends. The corresponding special-case subsets $\{NO_X'\}_L$

133 and $\{NO_X'\}_H$ of low and high NO_X' values from the whole time series $\{NO_X'\}$ of daily

134 fluctuations were then derived based on the predefined threshold values ($[NO_X']_L$ and $[NO_X']_H$,

135 correspondingly), marking the transition between clean ($[NO_X] \leq [NO_X']_L$) and polluted ($[NO_X]$

136 $\geq [NO_X']_H$) air.

137   Spatial localization of the origins of clean and polluted air at ZOTTO is performed

138 through the Condition Probability Function (CPF) analysis (Ashbaugh et al., 1985; Vasconcelos

139 et al., 1995). Residence times of air parcels associated with data samples from $\{NO_X'\}$, $\{NO_X'\}_L$

140 and $\{NO_X'\}_H$ are calculated on a regular 1°×1° grid as a number of trajectory segment endpoints

141 that fall into grid cells (g_{ij}, $g_{L,ij}$ and $g_{H,ij}$ values, correspondingly). The whole set of the grid cells

142 for which $g_{ij} > 0$ defines a region of influence constraining the spatial location of the gridded

143 emission sources that may be potentially significant for the ZOTTO site (Figure 1). The

144 conditional frequency $CF_{ij} = g^*_{ij} / g_{ij}$, where g^* stands for either g_L or g_H, gives then an estimate

145 of the probability that a $[NO_X']$ sample within the range of values from the special-case subset

146    $\{NO_X'\}_L$ or $\{NO_X'\}_H$ is related to the passage of air through the (ij)th cell, proved that the air has

147   actually passed through this cell (a conditional probability) on its way to the receptor site. Thus,

148   cells with high and statistically significant CF_{ij} values are indicative of areas of low and high

149   potential contributions to NO_X mixing ratios at ZOTTO in the case of $\{NO_X'\}_L$ and $\{NO_X'\}_H$

150   subsets, correspondingly.

151   The model-predicted origins of polluted air (source area for the site) and that of clean air

152   at ZOTTO were checked against the public databases on anthropogenic (EDGARv4.3.2, Figures

153   1a and 1b, see Janssens-Maenhout et al. (2019) for details) and wildfire (GFEDv4.1s, Figure 1c,

154   see Mu et al. (2011) and van der Werf et al. (2017)) NO_X emissions for a number of $[NO_X']_L$ and

155    $[NO_X']_H$ threshold values to assess the overall performance of the above CPF-based partitioning

156   of the air masses. Since major regional sources of pollutants are stationary in space and time or,

157   in the case of wildfires, have a distinct seasonal pattern, the origins of the above air masses are

158   expected to be different on a seasonal basis and conform with the spatial distribution of major

159   emission sources affecting the site, which provides an independent check for the correct choice

160   of the $[NO_X']_L$ and $[NO_X']_H$ values. We have found the NO_X' mixing ratios in the bottom and top

161   quartiles of $\{NO_X'\}$ to be nearly optimal for discriminating clean and polluted conditions,

162   correspondingly, with the remaining half of the observations left unclassified. In either case, the

163   origin of the air masses arriving at ZOTTO is identified as an area covered by a subset of grid

164   cells with $CF_{ij} > 0.25$, the expected conditional frequency in the absence of any association

165   between an air parcel trajectory path and the corresponding measured NO_x value from the

166   prescribed quartile of the data (Vasconcelos, 1995).

167

168
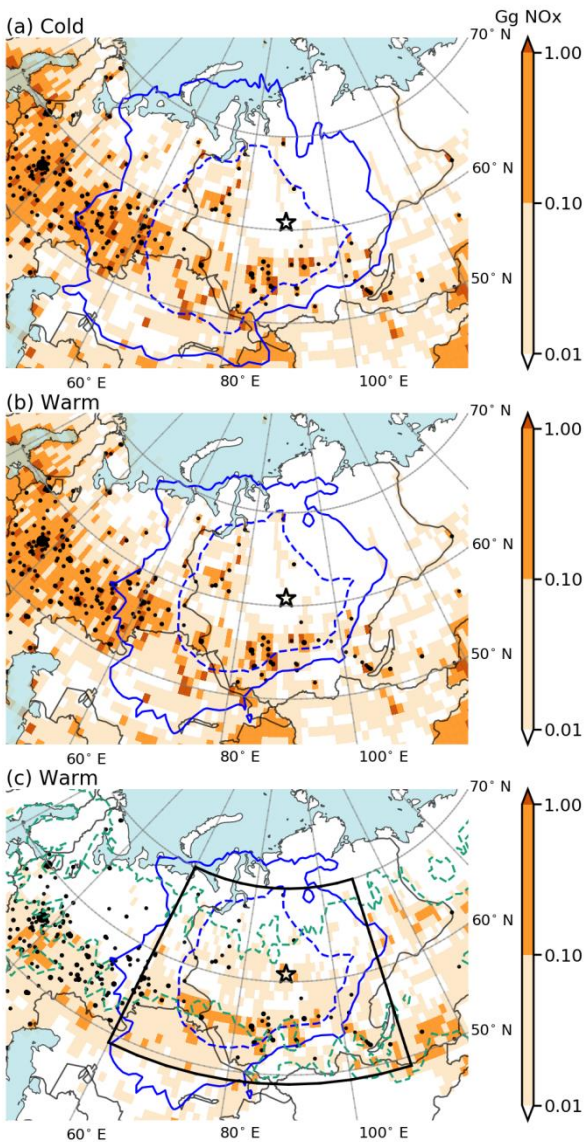
Figure 1. The region of influence for ZOTTO according to 3-day back trajectories. The g_{ij} values are normalized by the same values, calculated on the assumption that an air parcel arrives at ZOTTO from any direction with equal probability, to obtain $g_{NORM,ij}$ (Ashbaugh et al., 1985). The contours are $g_{NORM,ij} = 0.1$ (solid blue), $g_{NORM,ij} = 2.0$ (dashed blue). Color bar shows the monthly average **(a–b)** anthropogenic and **(c)** wildfire NO_X emissions ($\times 10^9$ g NO_X per month) on a $1^\circ \times 1^\circ$ latitude-longitude grid in **(a)** cold (October–March) and **(b–c)** warm (April–September) seasons of 2007–2014. Black dots are the cities with population $> 50\,000$ according to

176   naturalearthdata.com; star symbol is the ZOTTO site; green line is the area of boreal forest

177   according to the 1-km University of Maryland's Global Land Cover Classification (tree canopy

178   cover > 10%, canopy height > 5 m, see Hansen et al. (2000)); black rectangle in **(c)** is the region

179   for which total NO_X emissions are provided in Figure 4.

180   **4 Results**

181   4.1 O_3 and NO_X seasonal cycles

182   Average seasonal cycles of daily O_3 and NO_X levels at ZOTTO over the 2007–2014

183   observation period are shown in Figure 2, with the corresponding monthly statistics provided in

184   Table 1. The estimated annual means of daily O_3 and NO_X mixing ratios are 27.9 ppbv and 0.79

185   ppbv, correspondingly. The wide range of atmospheric transport pathways to the site (see Figure

186   1) and weather conditions, as well as different rates of photochemical processing of the polluted

187   air result in the observed strong short-term (synoptic) variability of daily O_3 and NO_X levels as

188   suggested by a large spread of the data within a month according to the monthly P05–P95

189   percentile range of daily mixing ratios. When averaged over all months of the observation

190   period, the amplitude of synoptic fluctuations for ozone, calculated as the P95–P05 difference, is

191   19.2 ppbv, which is comparable to the amplitude of the ozone seasonal cycle (22.6 ppbv) based

192   on the difference between O_3 median values of 42.3 ppbv in April and 19.7 ppbv in September.

193   The amplitude of ozone fluctuations is maximal from April to July (24.7 ppbv on average),

194   which is also the period of most intense photochemical ozone production from the regional

195   pollutant emissions (see more discussion below). Hence, weather-induced perturbations in local

196   ozone photochemistry are expected to be most important in the above months, resulting in the

197   observed seasonal increase in the total ozone variability at the site. One can see, however, that a

198   central annual tendency of the measured ozone levels at ZOTTO is a unimodal seasonal cycle

199   with a distinct maximum in April and a flat minimum in August–September. The similar ozone

200   cycle is typical for other background midlatitude sites in northwest Europe and North America

201   subjected to minor anthropogenic loading (Chan & Vet, 2010; Derwent et al., 2013; Katragkou et

202   al., 2015; Logan, 1985, 1989; Monks, 2000; Solberg et al., 1997; Vingarzan, 2004). Particularly,

203   the maximum value of 42.5 ppbv in April (Table 1) is very close to the annual maximum of

204   ozone at Mace Head (44 ppbv, see Derwent et al. (2013)) and rural Norwegian ozone monitoring

205   sites at similar latitudes (41–43 ppbv, 60°–65° N, see Solberg et al. (1997)).

206   Compared to the ozone data, a much higher degree of irregularity is observed for a

207 seasonal tendency of NO_X at the site, with the synoptic fluctuations clearly dominating the total

208 variability of daily NO_X levels (Figure 2b). Yet, a seasonal cycle of NO_X at the site is clearly

209 discernible, with monthly medians of NO_X peaking in the cold season from December to March

210 (0.95 ppbv on average) and reaching a minimum in late summer and early autumn (0.30 ppbv on

211 average for August–September). The observed accumulation of NO_X in a cold season replicates

212 the seasonal trends of other ozone precursor species (CO, CO_2, CH_4) at ZOTTO (Chi et al., 2013;

213 Lloyd et al., 2002; Timokhina et al., 2018) having large continental sources, whose lower-

214 tropospheric abundance is controlled to large extent by the seasonally varying vertical mixing

215 conditions and rates of photochemical destruction in CBL and the free troposphere aloft.

216 **Table 1.** Monthly Statistics of Average Afternoon (12:00–17:00 Local Time) O_3 and NO_x Mixing

217 Ratios at ZOTTO in Years 2007–2014 as Shown in Figure 2.

	O_3, ppb				NO_x, ppb			
	Mean	Median	P_{05}	P_{95}	Mean	Median	P05	P95
1	22.9	23.4	14.0	31.9	1.2	1.0	0.3	2.4
2	33.2	32.9	25.1	41.3	1.0	0.8	0.4	1.9
3	41.3	40.9	35.8	47.7	1.2	1.1	0.6	2.0
4	42.5	42.3	31.5	54.1	1.0	0.8	0.4	1.8
5	33.7	33.7	20.5	44.6	0.6	0.5	0.3	1.2
6	29.5	29.6	17.9	40.5	0.7	0.5	0.2	1.5
7	26.3	25.1	12.3	41.6	0.7	0.4	0.2	1.4
8	21.6	21.8	12.8	30.6	0.4	0.3	0.2	0.9
9	20.1	19.7	12.5	29.0	0.4	0.3	0.1	0.9
10	20.8	20.6	11.9	29.9	0.5	0.4	0.1	1.2
11	21.5	21.8	13.5	29.8	0.7	0.5	0.2	1.6
12	21.0	20.4	13.2	29.9	1.1	0.9	0.4	2.7
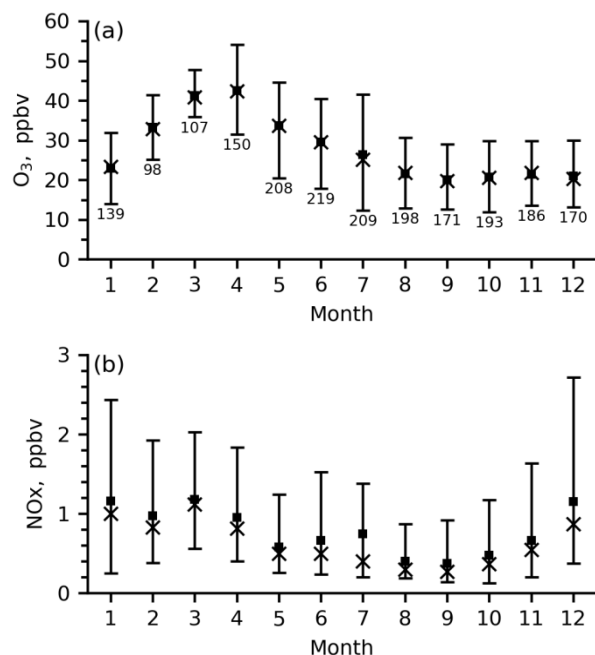
Figure 2. Monthly statistics of average afternoon (12:00–17:00 local time) **(a)** O_3 and **(b)** NO_X mixing ratios at ZOTTO for the 2007–2014 observation period: P05 and P95 percentiles (I), median (×), average (■), and the total number of observations per month for all years (labels).

4.2 O_3–NO_X correlations in warm and cold seasons

Figure 3a shows a significant positive correlation (R^2=0.55) between the daily mixing ratios of NO_X and O_3 in spring and summer. As far as a measured NO_X abundance at ZOTTO can be viewed as a proxy for the amount of NO_X emitted from upwind sources, the observed increase of daytime ozone with the in situ [NO_X] levels suggests a NO_X-controlled regime of photochemical ozone production within CBL on a regional scale in the above seasons. Since the [O_3] is proportional to log[NO_X], the rate of a local increase in O_3 mixing ratio ($\Delta[O_3] / \Delta[NO_X]$) is roughly inversely proportional to [NO_X] value. The latter can be explained on a qualitative basis by a lower efficiency of local photochemical ozone production from the oxidation of NMHCs per molecule of NO_X during daylight hours, as well as by incomplete photochemical processing of air at high NO_X levels, indicative of relatively short transport time to the site. A quadratic dependence of ozone on the logarithm of trajectory integrated NO_X emissions for a broad range of the equivalent [NO_X] values from <0.5 to ~10 ppbv has been proposed earlier by Solberg et al. (1997) to quantify the impact of upwind pollutant sources on ozone levels in the

236   polluted air arriving at Norwegian monitoring sites. Figure 3a also demonstrates that wildfires

237   immediately around ZOTTO, as is the case for the summer 2012, the severe fire season in

238   Siberia, strongly perturb ozone photochemistry resulting in a large scatter of data on the NO_X–O_3

239   plot. Also, for a fixed $[NO_X]$ value, daily ozone levels in fire-contaminated air seem to be

240   generally lower compared to the main body of the data evidencing for the suppressed ozone

241   production in smoke plumes from proximal fires. In a cold season from late autumn to early

242   winter, the linear least-squares fit of the daily data gives a weak but statistically significant

243   negative slope of -1.4 ppbv O_3 ppbv^{-1} NO_X, indicating net photochemical destruction of ozone in

244   polluted air via titration by NO_X and other co-emitted pollutants (Derwent et al., 1998; Parrish et

245   al., 1986; Solberg et al., 1997).

246
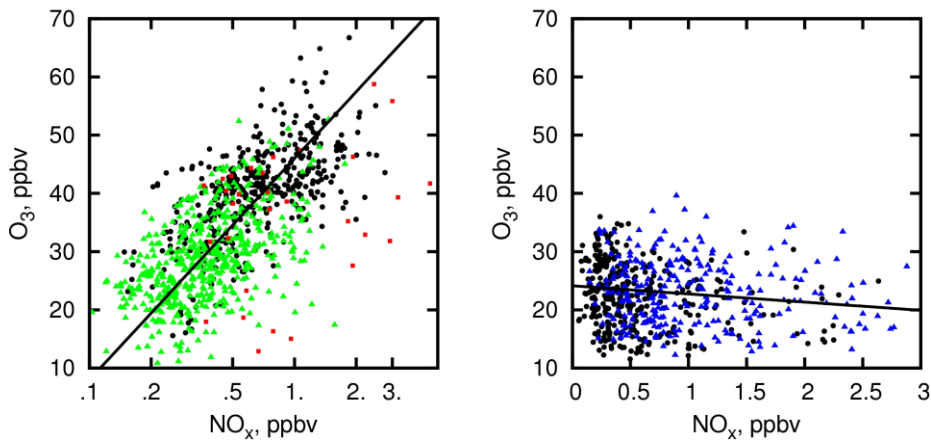
Figure 3. The O_3–NO_X dependence for the central months of each season of the 2007–2014

period: **(a)** April (black circles) and July (green triangles) data, $R^2 = 0.55$; **(b)** November (black

circles) and January (blue triangles) data, $R^2 = 0.02$. The orthogonal least squares fits (± 2

stdandard deviation) are: **(a)** $[O_3] = A + B \cdot \log_{10}([NO_X] / 1$ ppbv$)$, $A = 46.1$ (± 1.3) ppbv, $B = 37.8$

(± 3.4) ppbv; **(b)** $[O_3] = A - B \cdot [NO_X]$, $A = 24.1$ (± 1.2) ppbv, $B = 1.4$ (± 1.10) ppbv. The data

points for June–July 2012, the severe fire season in central Siberia, are shown by red squares and

are not used for the fitting.

254   4.3 Regional anthropogenic vs. fire-emitted NO_X

255   While the instantaneous photochemical ozone production at the measured NO_X mixing

256   ratios affects significantly the daytime ozone levels at ZOTTO (Moiseenko et al., 2019), the

257 observed correlation between daily afternoon NO_X and O_3 values reflects, in the most general

258 case, the cumulative effect of ozone chemistry in air mass during its transport from the source

259 area to the site as well. Previous studies (Michailov et al., 2017; Vasileva et al., 2011) show that

260 polluted air coming to the ZOTTO site contains commonly a mixture of fire-emitted and

261 anthropogenic pollutants whose individual contributions to the observed O_3 mixing ratios could

262 not be estimated unambiguously for an individual pollution event. Using g_{ij} values, we calculate

263 total monthly amounts of NO_X emissions in the source area for ZOTTO (see section 2.4) by

264 multiplying atmospheric residence time in the cell ($g_{ij} \cdot \Delta t$) by monthly NO_X emission (g NO_X per

265 hour per cell, see color bars in Figure 1) from either anthropogenic sources or wildfires and

266 summing the obtained values over all grid cells with nonzero g_{ij} values. The resulting monthly

267 anthropogenic and wildfire NO_X inputs ($E_{NOx,A}$ and $E_{NOx,F}$ values, correspondingly) are shown in

268 Figure 4. One can see that the anthropogenic NO_X represents the major fraction of the total

269 emitted NO_X in central North Eurasia (44°–70°N, 15°–130°E, Figure 4b) as well as within the

270 region of influence for the site (Figure 4c). The only exception is the summer months of the 2012

271 and 2013 severe wildfire years in central Siberia, when NO_X emissions from biomass burning

272 around the ZOTTO site greatly exceeded those from more distal anthropogenic sources. This is

273 contrasted to the regional CO emissions from wildfires which are comparable to, or an order of

274 magnitude higher, than the CO input from anthropogenic sources in years with moderate and

275 severe fire activity in Siberia, correspondingly (Mikhailov 2017; Shtabkin et al., 2016; Vasileva

276 et al., 2011).

277   The much higher regional anthropogenic input to the measured NO_X levels at ZOTTO

278 compared to the CO data results from low biomass burning emission factors for NO_X over a

279 range of biomes typical for Siberia, as well as the predominant pathways of atmospheric

280 transport to the site from the areas S and SW to the site characterized by the appreciable

281 anthropogenic load. We then try to separate the effects of total regional NO_X emissions on the

282 measured NO_X and O_3 levels at ZOTTO from the continental and hemispheric-scale effects of

283 transport and chemistry, which govern the observed O_3 and NO_X seasonal cycles, through

284 establishing the source-receptor relationship for the site and estimating the seasonal ozone

285 tendencies in clean and polluted conditions.

286
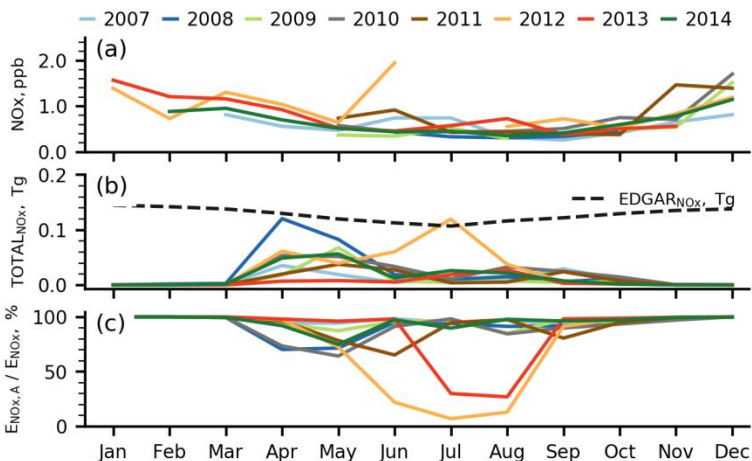
Figure 4. Seasonal variations of: **(a)** monthly mean NO_X (ppbv) at ZOTTO in 2007–2014; **(b)** total monthly biomass burning (GFEDv4.1s) and anthropogenic (EDGARv4.3.2) NO_X emissions (Tg) in central North Eurasia (49–70°N, 60–110°E, see Figure 1c); **(c)** fraction of anthropogenic NO_X input ($E_{NOx,A}/ (E_{NOx,A}+ E_{NOx,F})$) for the ZOTTO site.

4.4 Origins of clean and polluted air for the site

The gridded CF_{ij} fields calculated on a seasonal basis for the entire measurement period are shown in Figures 5 and 6 for polluted and clean conditions (as defined in section 2.4) at ZOTTO, correspondingly. The simulations were conducted for $\tau_t = 3$ days, which admits a nearly complete photochemical processing of air transported from the most distal pollution sources based on the reported *e*-folding times for NO_X species of 5–12 hours over remote continents, including boreal forests, during summer (Browne & Cohen, 2012) and 12–58 hours in winter under weakly polluted conditions (Kenagy et al., 2018). According to Figure 5, the polluted air is originated mostly from the areas of large anthropogenic NO_X emissions in southern Siberia, SE to W from the site, throughout the most time of year. Additionally, a contribution of more distal sources from the southern Ural Mountains and European Russia (i.e., the areas west of the 60° longitude) is seen distinctly in spring and fall due to more frequent zonal transport in these seasons. In summer, the statistically significant contribution of NO_X from wildfires in eastern Siberia E and NE to ZOTTO (Figure 1c) is well seen as the enclosed areas in Figure 5. This is consistent with the observed seasonal variations of wildfire activity in the region, which exhibits a marked latitudinal shift from the southern areas in spring and autumn to the central and northern parts of Siberia (> 60°N) in summer, following seasonal cycles of solar radiation and

308   precipitation in the region (Ponomarev et al., 2016; Vasileva et al., 2010). Noting the high

309   variability of wildfire emissions in space and time and the associated uncertainties in the

310   trajectory analysis, we consider the above spatial discrimination of the fire-related NO_X sources

311   as strong evidence for the overall consistency of all the assumptions underlying the CPF-based

312   approach. One can also see that the clean air originates mostly from continental areas with a

313   minor anthropogenic load (*remote areas* thereinafter) in the mid-to-high latitude belt 55°–70° N

314   (Figure 6), thus showing a distinct separation between the origins of clean and polluted air

315   masses. We then associate the above-defined clean and polluted conditions at ZOTTO with

316   continental baseline (CB), i.e., not subjected to the impact of regional pollution sources, and

317   regional emissions-influenced (REI) air masses to emphasize the regional extent of the derived

318   estimates. Alternatively, one could retain only the grid cells with statistically significant CF_{ij}

319   values according to the binomial test (Vasconcelos et al., 1995) or employ a more sophisticated

320   Kolmogorov-Zhurbenko low-pass filter (for details, see Vasileva et al. (2011) and references

321   therein) for the NO_X data to constrain the specified time range of the synoptic fluctuations, with

322   the main quantitative results of our analysis remaining essentially unchanged. Hence, the CPF-

323   based approach employed for the ZOTTO data analysis does provide robust constraints on the

324   source area of NO_X for the site and the ranges of observed NO_X levels that are representative of

325   clean and regionally polluted conditions.
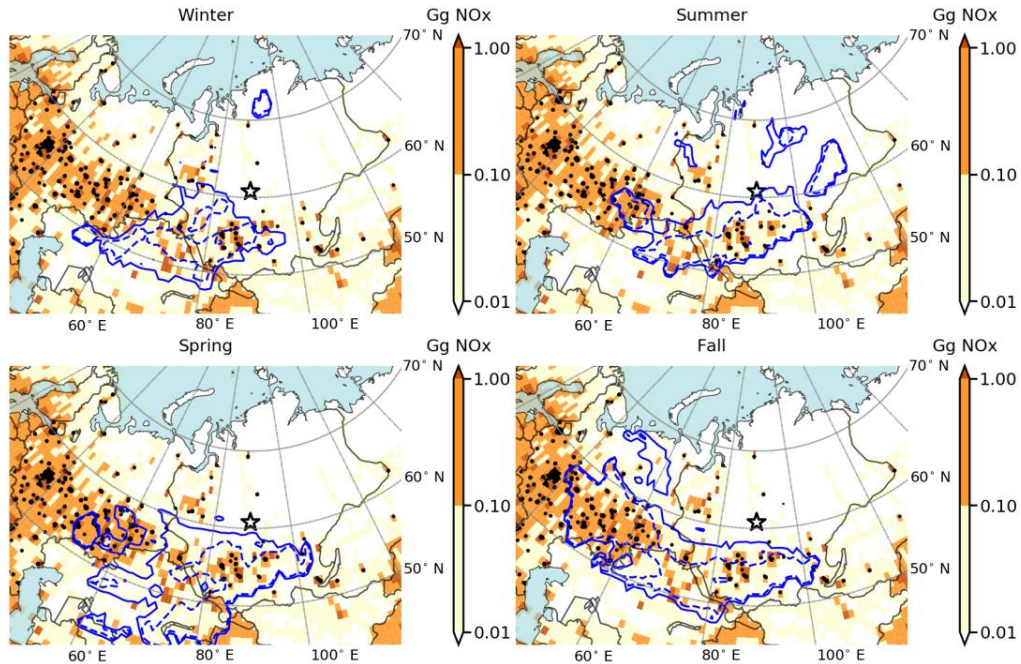
326   **Figure 5.** Conditional probability contours, CF = 0.25 (solid) and CF = 0.50 (dashed), for

327   ZOTTO against monthly average anthropogenic NO_X emissions for each season over years

328   2007–2014; CF_{ij} are calculated using the ensembles of 3-day back trajectories and high NO_X
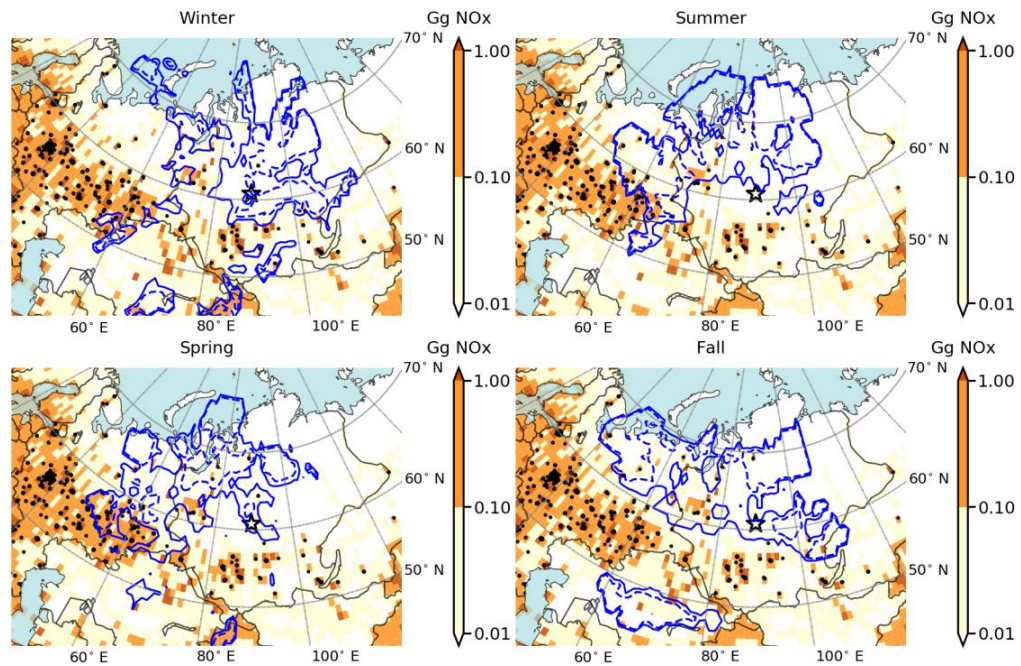
329   from top quartiles of the synoptic part of daytime (12:00–17:00 LT) average mixing ratios for

330   each season.

331   **Figure 6.** As Figure 5 but for the subset of NO_X data from the bottom quartile of the synoptic

332   part of daytime mixing ratios.

333   4.5 Seasonal variations of ozone in continental vs. NH midlatitude background air

334   By separating the air masses according to the measured NO_X mixing ratios, the overall

335   effect of regional pollution sources on the ozone levels at ZOTTO can be quantified on a

336   monthly basis. For each month of the observation period, mean daily ozone levels for CB and

337   REI air have been estimated based on the respective subsets of days from the month associated

338   with clean and polluted conditions, correspondingly. The derived monthly ozone data were used

339   to calculate the corresponding average and variability (min–max) interval for each month of a

340   year and air mass (Figure 7) for the years 2007–2014. Since each of the CB and REI data subsets

341   involves only a quarter of the original daily ozone data for each season, the monthly mean is

342   estimated using approximately seven daily ozone values on average. Also, significant gaps in the

343   original data affect the confidence of the derived 2007–2014 statistics for months with low data

344   coverage. Yet, the results obtained through separating ozone data into clean and polluted

345   categories according to the median of daily $[NO_X']$ values do not show much difference from

346   those shown in Figure 7. This supports the general notion that the derived average seasonal

347   cycles do provide a quantitative basis for comparing ozone levels in different air masses,

348   whereas the observed spread of monthly averages represents only some part of the total climatic

349   variability of ozone at the site. For comparison, we reproduce in Figure 7 the seasonal cycles of

350   monthly average ozone at the Mace Head (Ireland) atmospheric research station associated with

351   clean ("baseline" in the author's notation) air masses, transported mainly from central North

352   Atlantic, and the polluted air, transported from the western part of the European continent

353   ("European regionally polluted air"), as reported by Derwent et al. (2013). For brevity, we will

354   refer to the European origin of the polluted air measured at Mace Head as western Europe, yet

355   being aware of the site-specific pattern of the air transport climatology. As far as the amplitude

356   of the diurnal cycle of ozone at Mace Head is low throughout a year, reaching its maximum of an

357   order of a few ppbv in summer months (Tripathi et al., 2012), these measurements are probably

358   representative of average ozone values within the planetary boundary layer under well-mixed

359   conditions, thus allowing direct comparison against the afternoon ozone data at the ZOTTO site,

360   where ozone mixing ratios are subjected to strong diurnal variations in warm season from April

361   to September (Moiseenko et al., 2019). The Mace Head baseline ozone data have been identified

362   previously as representative of the Northern Hemisphere midlatitude background (NHMLB) air

363   to identify the European continent as a net source or sink for the tropospheric ozone on a

364   hemispheric scale (Derwent et al., 1998, 2013). Here we employ the ozone data at Mace Head

365   and ZOTTO for quantitative comparison of NHMLB and continental (CB and REI) air and the

366   assessment of the importance of Siberia for the midlatitude ozone budget.

367
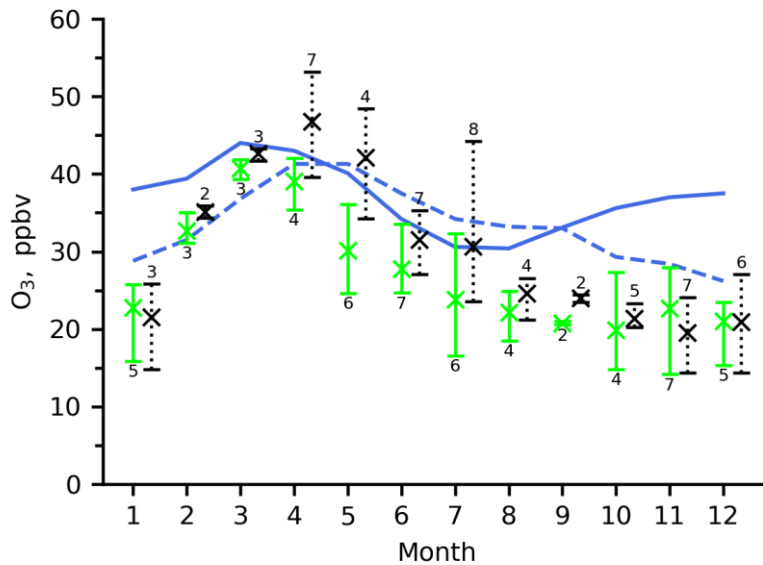
368

369   **Figure 7.** Seasonal dependence of daily (12:00–17:00) O_3 mixing ratios at ZOTTO for CB

370   (green) and REI (black) air masses (the 2007–2014 averages and min–max of monthly means);

371   labels give the number of monthly ozone data used for calculating statistics. The O_3 data points

372   for REI air are offset horizontally by 0.3 along the abscissa for better visibility. For comparison,

373   the 1987–2012 monthly mean O_3 levels in clean (solid blue line) and regionally polluted (dashed

374   blue line) air masses arriving from the European continent at the Mace Head station (53ºN, 10ºE,

375   25 m asl) are provided according to Derwent et al. (2013).

376   One can see from Figure 7 that ozone in NHMLB and CB air masses reaches its annual

377   maximum in March, with the 2007–2014 monthly average mixing ratio of 40.5 ppbv at ZOTTO

378   and about 44 ppbv at Mace Head. The observed marked similarity in the absolute value and time

379   of the ozone maximum for clean air at the two sites, which are highly different in meteorological

380   conditions and the origins of the measured air masses, strongly supports the earlier conclusion on

381   the polar front reservoir mechanism (Derwent et al., 1998; Monks, 2000; Penkett & Brice, 1986;

382   Vingarzan, 2004) as a common source for the early springtime ozone maximum both in the

383   maritime and continental boundary layer in the Northern Hemisphere midlatitudes.

384   Ozone levels in the European regionally polluted air exceed those in NHMLB air from

385   May to August, when the European region was found to represent a net source of tropospheric

386   ozone on the hemispheric scale (Derwent et al., 1998). A similar seasonal pattern of the

387   enhanced ozone levels in the polluted air is clearly seen for the ZOTTO site from February to

388   October, when ozone levels in REI air exceed those in CB air by up to 11 ppbv on average in

389   May. Hence, air pollutant emissions in Siberia provide a net source for ozone in CBL over

390   central North Eurasia for an appreciably longer period of year compared to the similar effect of

391   emissions for the region of western Europe. The prolonged period of net photochemical ozone

392   production in Siberia can be explained at least partially by substantially weaker anthropogenic

393   NO_X emissions in the region compared to those in western Europe and proportionally lower NO_X

394   levels in the CBL. During late winter and early spring under low solar radiation, the efficiency of

395   photochemical ozone production through the chemical chain reactions involving NO_X is

396   expected to be low under strongly limited tropospheric hydroxyl abundance, so that ozone

397   titration with NO_x still contributes to ozone destruction at a rate that is proportional to the

398   regional NO_X supply. Hence, low NO_X levels in the CBL are expected to result both in higher

399   efficiency of ozone production per NO_x molecule consumed (Liu et al., 1987) and less

400   importance of ozone sink via the chemical titration, resulting in net positive photochemical

401   ozone production in the Siberia region. This is contrasted to Mace Head and other rural

402   monitoring sites in northwest Europe, for which the titration process may still dominate over

403   ozone production owing to their proximity to the strong regional sources of ozone precursors

404   (Solberg et al., 1997). The earlier onset of the period of active ozone photochemistry in Siberia,

405   accompanied by ozone accumulation in CBL, explains the observed higher multi-year average

406   ozone levels in REI air in late winter and early spring compared to the respective ozone levels in

407   polluted air masses coming from western Europe to Mace Head, with the maximal difference

408   between average ozone levels for polluted air at the above sites of about 6 ppbv in April (Figure

409   7).

410   In Figure 7 one can see that multiyear average ozone levels in REI air exceed those in

411   NHMLB air in April–May by 3–5 ppbv. The regional pollutant emissions in Siberia provide then

412 a seasonal source for ozone in the midlatitude planetary boundary layer on the hemispheric scale

413 in these months. Additionally, high ozone levels are frequently observed in individual months of

414 the summer season in years where persistent anticyclonic weather conditions result in high

415 daytime air temperatures and solar radiation. Correspondingly, the multiyear average ozone

416 levels in REI air are seen to be close to ozone values in NHMLB air in June–July, as the ozone

417 statistics for these months are influenced by high monthly ozone values in individual years of the

418 2007–2014 period. In months of enhanced regional ozone production from April to July, for

419 which the highest difference between ozone abundance in REI and CB air is observed, monthly

420 ozone levels for REI air exceed NHMLB ozone levels in 13 of total 26 months of observations at

421 ZOTTO. The temperature-dependent regime of ozone photochemical production in REI air from

422 regional ozone precursors is clearly seen in Figure 8 which shows the 1.4 and 2.3 ppbv increase

423 in daytime ozone per °C for REI air in April–May and June–July, correspondingly. This can be

424 attributed to the combined effect of temperature-enhanced emissions of biogenic volatile organic

425 compounds (VOCs), soil emissions of NO_X, and organic reactivity, as well as to the increased

426 odd hydrogen production rate (through its dependence on UV radiation) from photolysis of

427 ozone and other species (Bowman & Seinfeld, 1994; Pusede et al., 2014; Romer et al., 2018;

428 Trainer et al., 1987a, 1987b) on the daytime surface ozone levels. High ozone formation

429 potential (OFP) due to the oxidation of biogenic VOCs over boreal forest areas of southern

430 Siberia is evidenced from the simultaneously measured VOCs, NO_X, and O_3 mixing ratios along

431 the Trans-Siberian Railroad in the summer of 2012 during the TROICA measurement campaign

432 (Skorokhod et al., 2017). Substantial increase in surface levels of both biogenic and total VOCs

433 with temperature was found for clean and regionally polluted air, with the highest mixing ratios

434 of isoprene and monoterpenes of 2–2.5 ppbv and 3–9 ppbv, correspondingly, observed under

435 high temperatures (> 28°C) and solar radiation. The average calculated OFP values (Carter,

436 1994; So & Wang, 2004) due to isoprene and monoterpenes in the region are about 15 and 18

437 ppbv of ozone, correspondingly, which compares well with the highest observed ozone

438 increments in REI air in summer (Figure 8b). It has been also found that, apart from large cities

439 and suburban areas, the contribution of anthropogenic VOCs to the local photochemical ozone

440 production in the Siberia region is generally not significant compared to that of biogenic VOCs,

441 leading to the overall conclusion on the primary role of biogenic VOCs in the regional ozone

442 balance (Berezina et al., 2019; Skorokhod et al., 2017).

443   The significant positive correlation of ozone with temperature ($R^2=0.35$) is seen in

444   summer for CB air as well (Figure 8b) and can be likely attributed to the pure effect of the

445   biogenic emissions of ozone precursors in clean CBL over the remote areas of Siberia. The

446   observed difference between the O_3–temperature slope rates in REI and CB air in summer (2.31

447   vs. 0.95 ppbv O_3 per °C) then quantifies a direct effect of anthropogenic and fire-emitted NO_X on

448   the net ozone production in addition to the temperature-controlled NO_X emissions from biogenic

449   sources. Statistically significant dependence of the CB ozone on temperature is absent for the

450   springtime data (Figure 8a) due to low seasonal temperatures and the associated biogenic

451   emissions.

452
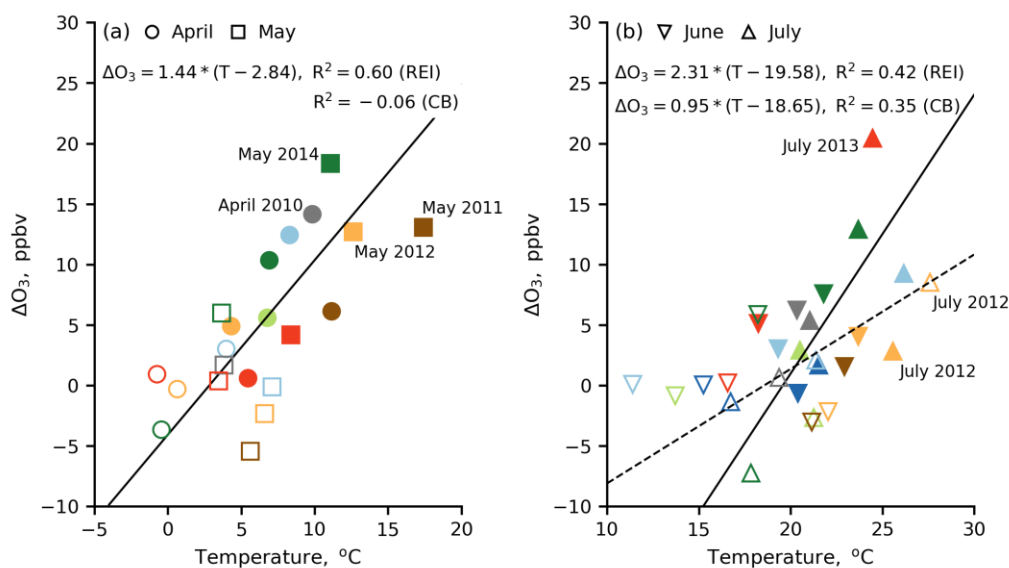
Figure 8. Difference between monthly daytime ozone value for the given air mass and the

454   corresponding 2007–2014 average ozone level for CB air vs. temperature in April–May (**a**) and

455   June–July (**b**) for CB (open) and REI (filled) air at ZOTTO. The lines give the linear, two-sided

456   regression fit to the REI (solid) and BC (dashed) ozone data.

457   Compared to the integrated effect of temperature on the regional ozone production, the

458   similar impact of wildfires seems to be more complicated owing to highly variable ozone

459   chemistry in biomass burning plumes resulting in suppressed ozone levels in a photochemically

460   young air vs. net ozone production on a later stage of plume evolution (Jaffe & Wigder, 2012;

461   Tanimoto et al., 2008). Both the effects are distinguished in ZOTTO data. Figure 8 shows a

462   negative difference between monthly ozone mixing ratios for REI and CB air of about 6 ppbv in

463   July 2012, a period of strong wildfires in central Siberia and directly around ZOTTO. This is

464   contrasted to strong wildfires in northern and central Siberia in July 2013 resulting in a monthly

465   ozone level of 45 ppbv, the highest ozone value over the 2007–2014 summer seasons. The ozone

466   value in July 2013 (Figure 8b, red triangle) is 20 and 14 ppbv higher compared to the multiyear

467   average ozone levels in CB and HNMLB air, correspondingly. A more straightforward

468   dependence of ozone on distal wildfires in southern Siberia and northern Kazakstan is found in

469   spring. Figure 8a shows the highest positive differences between ozone values for REI and CB

470   air of 13–18 ppbv for the months of severe wildfires (April 2010, May 2011, 2012, and 2014).

471   These are also the months of the highest springtime ozone values of 53 ppbv in April and up to

472   48 ppbv in May over the measurement period. We can finally conclude, based on the present

473   data, that severe wildfires in southern and central Siberia provide a net source for the midlatitude

474   ozone on the regional and global scales in a period from spring to early summer under favorable

475   weather conditions (see also Jaffe et al., 2004; Johnson et al., 2021; Lapina, 2009, and references

476   therein).

477   The seasonal cycle of the baseline ozone at Mace Head has a distinct minimum in July–

478   August, reflecting the transition from positive net photochemical ozone production in spring to

479   its destruction in summer within the maritime boundary layer (Derwent et al., 1998). This is

480   contrasted to the average CB ozone at ZOTTO, as well as ozone in the European polluted air at

481   Mace Head, which both show a monotonic decrease of monthly mean mixing ratios throughout

482   late spring and summer typical for other midlatitude weakly polluted sites (Katragkou et al.,

483   2015; Monks, 2000; Solberg et al., 1997) where ozone reaches its annual minimum in late

484   summer and early autumn. The marked qualitative similarity between the seasonal cycles of

485   ozone in CB air at ZOTTO and the polluted air from Europe at Mace Head evidences for a weak

486   persisting photochemical production of ozone during summer months in remote CBL owing to

487   biogenic and biomass burning emissions of ozone precursors which maintain background NO_X

488   and volatile organic compounds (VOC) at levels high enough for the net positive ozone

489   production in clean air. Yet, observations at ZOTTO show systematically lower ozone

490   abundance in CB air compared to that in NHMLB air, by approximately 5–15 ppbv from spring

491   to late autumn and by up to 18 ppbv in winter, reflecting the first-order effect of the surface

492   deposition process on the ozone balance in the region (Engvall-Stjernberg et al., 2012; Hirdman

493   et al., 2010). We then conclude finally that the regions of remote North Eurasia that are

494 associated with the CB air masses represent a net sink for ozone on a global scale throughout a

495 year, in close agreement with some previous studies (Engvall-Stjernberg et al., 2012; Paris et al.,

496 2010).

5 Conclusions

498   The source-receptor relationship of O_3 and NO_X for ZOTTO, a remote site in central

499 Siberia, has been examined for the observation period from March 2007 till December 2014

500 using the Conditional Probability Function analysis coupled with a back-trajectory model. Daily

501 ensembles of trajectories were assigned to the NO_X data, and the origins of polluted (REI) and

502 clean (CB) air masses carrying high and low NO_X to ZOTTO, correspondingly, were spatially

503 localized. The model-predicted source area of pollutant emissions affecting the ZOTTO site is

504 clearly associated with industrial regions of western Siberia and southern Ural Mountains,

505 whereas CB air originates mainly from remote areas of North Eurasia including north of

506 European Russia, central and northern Siberia within the 55°–70°N latitude belt. Additionally,

507 biomass burning NO_X emissions, of which the major part is emitted from wildfires in boreal

508 forests of the southern and central Siberia and steppe fires of northern Kazakhstan, contribute to

509 the regional NO_X input in severe fire seasons. Monthly ozone levels for REI air are found to be

510 higher by 7 ppbv on average in February – October and lower by 2 ppbv from November to

511 January than those for CB air, reflecting the seasonal change in ozone photochemistry from net

512 photochemical ozone production during most of the year to its destruction in winter in the

513 regionally-polluted air. The derived seasonal cycle of the CB ozone provides the most complete

514 determination of the near-surface ozone climatology for the remote central North Eurasia at the

515 given latitude and elevation.

516   The ozone seasonal cycles at ZOTTO and Mace Head (Ireland), a remote monitoring site

517 measuring ozone levels at the western inflow boundary of the continent, were compared to assess

518 the relative importance of central North Eurasia as a net source or sink of the tropospheric ozone

519 on the regional and global scales. The ozone seasonal maxima at both the sites are observed in

520 March and April for clean and regionally polluted air, correspondingly. This evidences of a

521 common hemispheric-wide source for the springtime ozone maxima at the two sites, upon which

522 a regional effect of ozone precursor emissions is superimposed. Essentially, the period of net

523 photochemical ozone production in the regionally polluted air at ZOTTO is observed for a

524 substantially longer period (from February to October) compared to the similar period at Mace

525 Head lasting from May to August. The observed difference can be explained by the proximity of

526 major regional sources of atmospheric pollutants to the Mace Head site. Additionally, lower

527 atmospheric NO_X input from regional sources in Siberia compared to that in western Europe

528 results in higher efficiency of ozone production per a molecule NO_X consumed under the regime

529 of hydroxyl-limited ozone formation during months with low solar radiation.

530   Our results agree with the general conclusion of previous studies (Engvall-Stjernberg et

531 al., 2012; Paris et al., 2010; Thorp et al., 2020) that surface ozone in the region of observations is

532 controlled mainly by the balance between regional anthropogenic emissions and seasonally

533 varying processes of atmospheric transport and surface deposition. Consequently, the ozone

534 levels in CB air are found to be substantially less than those for clean air masses at Mace Head

535 throughout a year. The remote central North Eurasia represents then a sink for ozone in the

536 boundary layer throughout a year on the hemispheric scale.

537   In late spring (April–May), regional anthropogenic and wildfire emissions provide a

538 seasonal source for ozone in CBL over Siberia, resulting in ozone levels well exceeding those

539 observed in the continental baseline and the Northern Hemisphere midlatitude background air

540 according to the Mace Head data. In summer, hot weather conditions accompanied by high UV

541 radiation are favorable for enhanced photochemical ozone production in REI air from the

542 regional ozone precursors, with monthly ozone levels in polluted air greatly exceeding those in

543 CB and NHMBL air masses. Throughout the most photochemically active period of a year from

544 April to July, the highest ozone levels are observed in years of strongest fire activity, where the

545 combined effect of anthropogenic and temperature-enhanced biogenic emissions of VOCs and

546 NO_X is amplified by wildfire emissions of ozone precursors. Consequently, one can expect that

547 in individual years of persisting anticyclonic weather and accompanying strong fire activity, the

548 regions of southern and central Siberia represent a net source for ozone on the hemispheric scale

549 during summer months as well.

550 **Acknowledgments**

23

568   **References**

569   Arnold, S. R., Lombardozzi, D., Lamarque, J. F., Richardson, T., Emmons, L. K., Tilmes, S., et

570   al. (2018), Simulated global climate response to tropospheric ozone-induced changes in plant

571   transpiration. Geophysical Research Letters, 45(23), 13070-13079.

572   https://doi.org/10.1029/2018GL079938

573   Ashbaugh, L. L., Malm, W. C., & Sadeh, W. D. (1985), A residence time probability analysis of

574   sulfur concentrations at Grand Canyon National park. Atmospheric Environment 19, 1263-1270.

575   https://doi.org/10.1016/0004-6981(85)90256-2

576   Atkinson, R. W., Butland, B. K., Dimitroulopoulou, C., Heal, M. R., Stedman, J. R., Carslaw, N.,

577   et al. (2016), Long-term exposure to ambient ozone and mortality: A quantitative systematic

578   review and meta-analysis of evidence from cohort studies. BMJ Open, 6(2), 1–10.

579   https://doi.org/10.1136/bmjopen-2015-009493

580   Berezina, E. V., Moiseenko, K. B., Skorokhod, A. I., & Elanskii, N. F. (2017), Aromatic volatile

581   organic compounds and their role in ground-level ozone formation in Russia. Doklady Earth

582   Science, 474, 599–603. https://doi.org/10.1134/S1028334X1705021X

583 Bowman, F. M., & Seinfeld, J. H. (1994), Ozone productivity of atmospheric organics. Journal

584 of Geophysical Research, 99(D3), 5309-5324. https://doi.org/10.1029/93JD03400

585 Browne, E. C., & Cohen, R. C. (2012), Effects of biogenic nitrate chemistry on the NOx lifetime

586 in remote continental regions. Atmospheric Chemistry and Physics, 12, 11917–11932.

587 https://doi.org/10.5194/acp-12-11917-2012

588 Cailleret, M., Ferretti, M., Gessler, A., Rigling, A., & Schaub, M. (2018), Ozone effects on

589 European forest growth – Towards an integrative approach. Journal of Ecology, 106, 1377–1389.

590 https://doi.org/10.1111/1365-2745.12941

591 Carter, W. P. L. (1994), Development of ozone reactivity scales for volatile organic compounds,

592 Journal of the Air & Waste Management Association, 44(7), 881–899.

593 https://doi.org/10.1080/1073161X.1994.10467290

594 Chan, E., & Vet, R. J. (2010), Baseline levels and trends of ground level ozone in Canada and

595 the United States. Atmospheric Chemistry Physics, 10, 8629–8647. https://doi.org/10.5194/acp-

596 10-8629-2010

597 Chi, X., Winderlich, J., Mayer, J.-C., Panov, A. V., Heimann, M., Birmili, W., et al. (2013),

598 Long-term measurements of aerosol and carbon monoxide at the ZOTTO tall tower to

599 characterize polluted and pristine air in the Siberian taiga. Atmospheric Chemistry and Physics,

600 13, 12271–12298. https://doi.org/10.5194/acp-13-12271-2013

601 Derwent, R. G., Manning, A. J., Simmonds, P. G., Spain, T. G., & O'Doherty, S. (2013),

602 Analysis and interpretation of 25 years of ozone observations at the Mace Head Atmospheric

603 Research Station on the Atlantic Ocean coast of Ireland from 1987 to 2012. Atmospheric

604 Environment, 80, 361–368. https://doi.org/10.1016/j.atmosenv.2013.08.003

605 Derwent, R. G., Simmonds, P. G., & Collins, W. J. (1994), Ozone and carbon monoxide

606 measurements at a remote maritime location, Mace Head, Ireland, from 1990 to 1992.

607 Atmospheric Environment, 28(16), 2623–2637. https://doi.org/10.1016/1352-2310(94)90436-7

608 Eneroth, K., Kjellstrom, E., & Holmen, K. (2003), Interannual and seasonal variations in

609 transport to a measuring site in western Siberia and their impact on the observed atmospheric

610 CO2 mixing ratio. Journal of Geophysical Research, 108(D21), 4660.

611 https://doi.org/doi:10.1029/2002JD002730

612   Engvall-Stjernberg, A.-C , Skorokhod, A. I., Elansky, N. F., Paris, J.-D , Nédélec, P., & Stohl.,

613   A. (2012), Low surface ozone in Siberia. Tellus B, 64, 11607.

614   https://doi.org/10.3402/tellusb.v64i0.11607

615   Felzer, B. S., Cronin, T. W., Melillo, J. M., Kicklighter, D. W., & Schlosser,C. A. (2009),

616   Importance of carbon-nitrogen interactions and ozone on ecosystem hydrology during the 21st

617   century. Journal of Geophysical Research, 114, G01020. https://doi.org/10.1029/2008JG000826

618   Fuhrer, J. (2009), Ozone risk for crops and pastures in present and future climates.

619   Naturwissenschaften, 96(2), 173–194. https://doi.org/10.1007/s00114-008-0468-7

620   Hansen, M., DeFries, R., Townshend, J. R. G., & Sohlberg, R. (2000), Global land cover

621   classification at 1 km resolution using a decision tree classifier. International Journal of Remote

622   Sensing, 21(6–7), 1331–1364. https://doi.org/10.1080/014311600210209

623   Heimann, M., Schulze, E. D., Winderlich, J., Andreae, M. O., Chi, X., Gerbig, C., et al. (2014),

624   The Zotino Tall Tower Observatory (Zotto): Quantifying large scale biogeochemical changes in

625   Central Siberia. Nova Acta Leopoldina, 117(399), 51-64.

626   Hirdman, D., Sodermann, H., Eckhardt, S., Burkhart, J. F, Jefferson, A., Mefford, T., et al.

627   (2010), Source identification of short-lived air pollutants in the Arctic using statistical analysis of

628   measurement data and particle dispersion model output. Atmospheric Chemistry and Physics, 10,

629   669–693. https://doi.org/10.5194/acp-10-669-2010

630   Hollaway, M. J., Arnold, S. R., Challinor, A. J., & Emberson, L. D. (2012), Intercontinental

631   trans-boundary contributions to ozone-induced crop yield losses in the Northern Hemisphere.

632   Biogeosciences, 9(1), 271– 292. https://doi.org/10.5194/bg-9-271-2012.

633   Jaffe, D. A., Bertschi, I., Jaeglé, L., Novelli, P., Reid, J.S., Tanimoto, H., et al. (2004), Long-

634   range transport of Siberian biomass burning emissions and impact on surface ozone in western

635   North America. Geophysical Research Letters, 31(16), 6-9.

636   https://doi.org/10.1029/2004GL020093

637   Jaffe, D. A., & Wigder, N. L. (2012), Ozone production from wildfires: A critical review.

638   Atmospheric Environment, 51, 1–10. https://doi.org/10.1016/j.atmosenv.2011.11.063

639   Janssens-Maenhout, G., Crippa, M., Guizzardi, D., Muntean, M., Schaaf, E., Dentener, F., et al.

640   (2019), EDGAR v4.3.2 Global Atlas of the three major greenhouse gas emissions for the period

641 1970–2012. Earth System Science Data, 11(3), 959-1002. https://doi.org/10.5194/essd-11-959-
642 2019

643 Johnson, M. S., Strawbridge, K., Knowland, K. E., Keller, C., & Travis, M. (2021), Long-range
644 transport of Siberian biomass burning emissions to North America during FIREX-AQ.
645 Atmospheric Environment, 118241. https://doi.org/10.1016/j.atmosenv.2021.118241

646 Katragkou, E., Zanis, P., Tsikerdekis, A., Kapsomenakis, J., Melas, D., Eskes, H., et al. (2015),
647 Evaluation of near-surface ozone over Europe from the MACC reanalysis. Geoscientific Model
648 Developement, 8, 2299–2314. https://doi.org/10.5194/gmd-8-2299-2015

649 Kenagy, H. S., Sparks, T. L., Ebben, C. J., Wooldrige, P. J., Lopez-Hilfiker, F. D., Lee, B. H., et
650 al. (2018), NOx lifetime and NOy partitioning during WINTER. Journal of Geophysical
651 Research, 123, 9813– 9827. https://doi.org/10.1029/2018JD028736

652 Kleinman, L. I., Daum, P. H., Lee, J. H., Lee, Y., Nunnermacker, L. J., Stephen, R.S., et al.
653 (1997), Dependence of ozone production on NO and hydrocarbons in the troposphere,
654 Geophysical Research Letters, 101(18), 2299–2302. https://doi.org/10.1029/97GL02279

655 Kotelnikov, S. N., Stepanov, E. V., & Ivashkin, V.T. (2017), Ozone concentration in the ground
656 atmosphere and morbidity during extreme heat in the summer of 2010, Doklady Biological
657 Sciences, 473(1), 64–68. https://doi.org/10.1134/S0012496617020107

658 Kozlova, E. A., & Manning, A. C. (2009), Methodology and calibration for continuous
659 measurements of biogeochemical trace gas and O2 concentrations from a 300-m tall tower in
660 central Siberia. Atmospheric Measurement Techniques, 2(1), 205-220.
661 https://doi.org/10.5194/amt-2-205-2009

662 Lapina, K., (2009). Boreal forest fire impacts on lower troposphere carbon monoxide and ozone
663 levels at the regional to hemispheric scales, (Doctoral dissertation). Retrieved from Digital
664 Commons – Michigan Tech. (https://doi.org/10.37099/mtu.dc.etds/712). Houghton, MI:
665 Michigan Technological University.

666 Lin, X., Trainer, M., & Liu, S. C. (1988), On the nonlinearity of the tropospheric ozone
667 production. Journal of Geophysical Research, 93(D12), 15879–15888.
668 https://doi.org/10.1029/JD093iD12p15879

669　Liu, F., Beirle, S., Zhang, Q., Dörner, S., He, K., and Wagner, T. (2016), NOx lifetimes and

670　emissions of cities and power plants in polluted background estimated by satellite observations.

671　Atmospheric Chemistry and Physics, 16, 5283–5298. https://doi.org/10.5194/acp-16-5283-2016

672　Liu, S. C., Trainer, M., Fehsenfeld, F. C., Parrish, D. D., Williams, E. J., Fahey, D. W., et al.

673　(1987), Ozone production in the rural troposphere and the implications for regional and global

674　ozone distributions. Journal of Geophysical Research, 92, 4191–4207.

675　https://doi.org/10.1029/JD092iD04p04191

676　Lloyd, J., Langenfelds, R. L., Francey, R. J., Gloor, M., Tchebakova, N. M., Zolotoukhine, D., et

677　al. (2002), A trace-gas climatology above Zotino, central Siberia. Tellus B, 54(5), 749-767.

678　https://doi.org/10.3402/tellusb.v54i5.16726

679　Logan, J. A. (1985), Tropospheric ozone: seasonal behavior, trends and anthropogenic influence.

680　Journal of Geophysical Research, 90(10), 463–482. https://doi.org/10.1029/JD090iD06p10463

681　Logan, J. A. (1989), Ozone in rural areas of the United States. Journal of Geophysical Research,

682　94(D6), 8511–8532. https://doi.org/10.1029/JD094iD06p08511

683　Mikhailov, E. F., Mironova, S., Mironov, G., Vlasenko, S., Panov, A., Chi, X., et al. (2017),

684　Long-term measurements (2010–2014) of carbonaceous aerosol and carbon monoxide at the

685　Zotino Tall Tower Observatory (ZOTTO) in central Siberia. Atmospheric Chemistry and

686　Physics, 17(23), 14365-14392. https://doi.org/10.5194/acp-17-14365-2017

687　Mills, G., Hayes, F., Simpson, D., Emberson, L., Norris, D., Harmens, H., Büker, P. (2011),

688　Evidence of widespread effects of ozone on crops and (semi-)natural vegetation in Europe

689　(1990–2006) in relation to AOT40- and flux-based risk maps. Global Change Biology 17(1),

690　592-613. https://doi.org/10.1111/j.1365-2486.2010.02217.x

691　Moiseenko, K. B., Berezina, E. V., Vasileva, A. V., Shtabkin., Y. A., Skorokhod., A. I., Elanskii,

692　& N. F., Belikov, I. B. (2019), Nhe NOx-limiting regime of photochemical ozone generation in a

693　weakly polluted convective boundary layer: Observations at the ZOTTO tall tower observatory

694　in central Siberia, 2007–2015. Doklady Earth Sciences, 487(2), 981–985.

695　https://doi.org/10.1134/S1028334X19080282

696　Monks, P. S. (2000), A review of the observations and origins of the spring ozone maximum.

697　Atmospheric Environment, 34(21), 3545–3561. https://doi.org/10.1016/S1352-2310(00)00129-1

698   Monks ,P. (2005), Gas-phase radical chemistry in the troposphere. Chemical Society Reviews,

699   34(5), 376-395. https://doi.org/10.1039/b307982c

700   Mills, G., Buse, A., Gimeno, B., Bermejo, V., Holland, M., Emberson, L., & Pleijel, H. (2007),

701   A synthesis of AOT40-based response functions and critical levels of ozone for agricultural and

702   horticultural crops. Atmospheric Environment, 41, 2630–2643.

703   Mu, M., Randerson, J. T., van der Werf, G. R., Giglio, L., Kasibhatla, P., Morton, D., et al.

704   (2011), Daily and 3-hourly variability in global fire emissions and consequences for atmospheric

705   model predictions of carbon monoxide, Journal of Geophysical Research, 116(D24),

706   https://doi.org/10.1029/2011JD016245

707   Oltmans, S. J. (1981), Surface ozone measurements in clean air, Journal of Geophysical

708   Research, 86(C2), 1174– 1180, https://doi.org/10.1029/JC086iC02p01174

709   Paris, J.-D., Stohl, A., Ciais, P., Nédélec, P., Belan. B. D., Arshinov, M., Yu., & Ramonet, M.

710   (2010), Source-receptor relationships for airborne measurements of CO2, CO and O3 above

711   Siberia: a cluster-based approach. Atmospheric Chemistry and Physics, 10, 1671–1687.

712   https://doi.org/10.5194/acp-10-1671-2010

713   Parrish, D. D., Fahey, D. W., Williams, E. J., Liu, S. C., Trainer, M., Murphy, P. C., et al.

714   (1986), Background ozone and anthropogenic ozone enhancement at niwot ridge, Colorado.

715   Journal of Atmospheric Chemistry, 4, 63–80. https://doi.org/10.1007/BF00053773

716   Parrish, D. D., Holloway, J. S., Trainer, M., Murphy, P. C., Forbes, G. L., Fehsenfeld, F. C.,

717   &Forbes, G. L. (1993), Export of North American ozone pollution to the North Atlantic Ocean,

718   Science, 259(5100), 1436-1439. https://doi.org/10.1126/science.259.5100.1436

719   Parrish, D. D., Law, K. S., Staehelin, J., Derwent, R., Cooper, O. R., Tanimoto, H., et al. (2013),

720   Lower tropospheric ozone at northern midlatitudes: Changing seasonal cycle. Geophysical

721   Research Letters, 40(8), 1631–1636, https://doi.org/10.1002/grl.50303

722   Penkett, S. A., & Brice, K. A. (1986), The spring maximum in photo-oxidants in the Northern

723   Hemisphere. Nature 319, 655-657. https://doi.org/10.1038/319655a0

724   Pusede, S. E., Gentner, D. R., Wooldridge, P. J., Browne, E. C., Rollins, A. W., Min, K.-E., et al.

725   (2014), On the temperature dependence of organic reactivity, nitrogen oxides, ozone production,

726 and the impact of emission controls in San Joaquin Valley, California. Atmospheric Chemistry

727 and Physics, 14, 3373–3395. https://doi.org/10.5194/acp-14-3373-2014

728 Singh, H. B., Ludwig, F. L., & Johnson, W. B. (1978), Tropospheric Ozone: Concentrations and

729 variabilities in clean remote atmospheres. Atmospheric Environment, 12(11), 2185–2196.

730 https://doi.org/10.1016/0004-6981(78)90174-9

731 Skorokhod, A. I., Berezina, E. V., Moiseenko, K. B., Elansky, N. F., Belikov, I. B. (2017),

732 Benzene and Toluene in the surface air of North Eurasia from TROICA-12 campaign along the

733 Trans-Siberian railway. Atmospheric Chemistry and Physics, 17, 5501-5514. doi: 10.5194/acp-

734 17-5501-2017

735 Romer, P. S., Duffey, K. C., Wooldridge, P. J., Edgerton, E., Baumann, K., Feiner, P. A., et al.

736 (2018), Effects of temperature-dependent NOx emissions on continental ozone production,

737 Atmospheric Chemistry and Physics, 18, 2601–2614. https://doi.org/10.5194/acp-18-2601-2018

738 So, K. L., & Wang T. (2004), C3-C12 non-methane hydrocarbons in subtropical Hong Kong:

739 spatial-temporal variations, source-receptor relationships and photochemical reactivity. Science

740 of The Total Environment, 328(1–3), 161–174. https://doi.org/10.1016/j.scitotenv.2004.01.029

741 Solberg, S., Stordal, F. & Hov, ø. (1997), Tropospheric ozone at high latitudes in clean and

742 polluted air masses, a climatological study. Journal of Atmospheric Chemistry, 28, 111–123.

743 https://doi.org/10.1023/A:1005766612853

744 Tanimoto, H., Matsumoto, K., & Uematsu, M. (2008), Ozone-CO correlations in Siberian

745 wildfire plumes observed at Rishiri Island. SOLA, 4, 65–68.

746 https://doi.org/10.2151/SOLA.2008-017

747 Thorp, T., Arnold, S. R., Pope, R. J., Spracklen, D. V., Conibear, L., Knote, C., et al. (2020),

748 Late-Spring and Summertime Tropospheric Ozone and NO2 in Western Siberia and the Russian

749 Arctic: Regional Model Evaluation and Sensitivities. Atmospheric Chemistry and Physics.

750 https://doi.org/10.5194/acp-2020-426

751 Timokhina, A. V., Prokushkin, A. S., Panov, A. V., Kolosov, R. A., Sidenko, N. V., Lavric, J.

752 V., & Heimann, M. (2018), Interannual variability of atmospheric CO2 concentrations over

753 central Siberia from ZOTTO data for 2009–2015. Russian Meteorology and Hydrology, 43(5),

754 288-294. https://doi.org/10.3103/S1068373918050023.

755 Trainer, M., Hsie, E. Y., McKeen, S. A., Tallamraju, R., Parrish, D. D., Fehsenfeld, F. C., & Liu,

756 S. C. (1987b), Impact of natural hydrocarbons on hydroxyl and peroxy radicals at a remote site,

757 Journal of Geophysical Research, 92(D10), 11879– 11894. doi:10.1029/JD092iD10p11879

758 Trainer, M., Williams, E., Parrish, D., Buhr, M. P., Allwine, E. J., Westberg, H. H., et al.

759 (1987a), Models and observations of the impact of natural hydrocarbons on rural ozone. Nature

760 329, 705–707. https://doi.org/10.1038/329705a0

761 Tripathi, O. P., Jennings, S. G. , O'Dowd, C., O'Leary, B., Lambkin, K., Moran, E., et al. (2012),

762 An assessment of the surface ozone trend in Ireland relevant to air pollution and environmental

763 protection. Atmospheric Pollution Research, 3(3), 341–351.

764 https://doi.org/10.5094/APR.2012.038

765 Turner, M. C., Jerrett, M., Pope, C. A., Krewski, D., Gapstur, S. M., Diver, W. R., et al. (2016),

766 Long-term ozone exposure and mortality in a large prospective study. American Journal of

767 Respiratory and Critical Care Medicine, 193(10), 1134–1142.

768 https://doi.org/10.1164/rccm.201508-1633OC

769 van der Werf, G. R., Randerson, J. T., Giglio, L., van Leeuwen, T. T., Chen, Y., Rogers, B. M.,

770 et al. (2017), Global fire emissions estimates during 1997–2016. Earth System Science Data, 9,

771 697–720, https://doi.org/10.5194/essd-9-697-2017

772 Vasconcelos, L. A. P., Kahl, J. D. W., Liu, D., Macias, E. S., & White, W. H. (1996), A tracer

773 calibration of back trajectory analysis at the Grand Canyon, Journal of Geophysical Research,

774 101(D14), 329– 19,335, https://doi.org/10.1029/95JD02609

775 Vasileva, A. V., Moiseenko, K. B., Mayer, J.-C., Jürgens, N., Panov, A., Heimann, M., &

776 Andreae, M. O. (2011), Assessment of the regional atmospheric impact of wildfire emissions

777 based on CO observations at the ZOTTO tall tower station in central Siberia. Journal of

778 Geophysical Research, 116(D07301). https://doi.org/10.1029/2010JD014571

779 Vingarzan, R. (2004), A review of surface ozone background levels and trends. Atmospheric

780 Environment, 38, 3431–3442. https://doi.org/10.1016/j.atmosenv.2004.03.030